Charge transport properties of bulk Ta_3N_5 from first principles

Juliana M. Morbec* and Giulia Galli
Institute for Molecular Engineering, University of Chicago, Chicago, Illinois 60637, USA
(Received 28 September 2015; revised manuscript received 15 December 2015; published 6 January 2016)

Tantalum nitride is considered a promising material for photoelectrochemical water splitting, however, its charge transport properties remain poorly understood. We investigated polaronic and band transport in Ta_3N_5 using first-principles calculations. We first studied the formation of small polarons using density-functional theory (DFT) including DFT + U and hybrid functionals. We found that electron small polarons may occur but hole polarons are not energetically favorable. The estimated polaronic mobility for electrons is at least three orders of magnitude smaller than that measured in Ta_3N_5 films, suggesting that the main transport mechanism for both electrons and holes is bandlike. Since band transport is strongly affected by the carrier effective masses, and Ta_3N_5 is known to have large electron and hole effective masses, we also investigated whether substitutional impurities or strain may help lower the effective masses. We found a significant reduction in both electron and hole effective masses (up to 17% for electrons and 39% for holes) under applied strain, which may lead to a substantial improvement (up to 30% for electrons and 15% for holes) in the carrier mobilities.

DOI: 10.1103/PhysRevB.93.035201

I. INTRODUCTION

Tantalum nitride (Ta_3N_5) is considered to be a promising material for photoelectrochemical water splitting due to its suitable band gap (∼2.1 eV) [1–3] for visible light absorption and favorable band edge alignments for both hydrogen and oxygen evolution reactions [3]. However, recent experiments have reported a low photocurrent and a poor overall performance of Ta_3N_5 photoanodes for water oxidation [4,5], which is likely caused by poor charge transport properties [6–8] as well as by rapid photodegradation of the samples in water [5,9].

Recently, using first-principles calculations, we computed the effective masses of holes and electrons in bulk Ta_3N_5 [8], which were found to be large along several directions, e.g., $2.70m_0$ for electrons and $3.56m_0$ for holes along the ΓY direction [8]; these values are significantly larger, for example, than those computed for the hybrid organic-inorganic perovskites $CH_3NH_3PbI_3$, considered to be materials with high carrier mobilities [10,11]: $m_e = 0.09$–$0.26m_0$ and $m_h = 0.08$–$0.31m_0$. Our results suggested that Ta_3N_5 may have low carrier mobilities and hence unfavorable bulk charge transport properties. We also found that the effective masses of holes are larger (up to ∼3 times) than those of electrons in most directions, indicating that holes may have a lower mobility; this is consistent with the experimental finding of Pinaud *et al.* [6], who reported that hole transport plays a major role in the poor photoactivity of Ta_3N_5 photoanodes. Carrier mobilities of electrons in Ta_3N_5 films were recently measured by Ziani *et al.* [7] and Respinis *et al.* [12]. For the monoclinic phase of Ta_3N_5, Ziani *et al.* [7] obtained electron mobilities in the range of 1.3–4.4 cm^2/V s—as low as those reported for other photoanode materials, such as Fe_2O_3 (1.53 cm^2/V s) [13]) and TiO_2 (0.1–4 cm^2/V s) [14]—and lifetimes of electrons in the range of 3.1–8.7 ps, a few orders of magnitude lower than that reported, e.g., for $BiVO_4$ (∼40 ns) [15]. For the orthorhombic phase of Ta_3N_5, Respinis *et al.* [12] found electron mobilities of 1.0×10^{-1} cm^2/V s.

Hence, understanding the charge transport mechanisms in Ta_3N_5 is key in improving its performance for photoelectrochemical water splitting. In this paper we used first-principles calculations based on density-functional theory to study the charge transport properties of bulk Ta_3N_5. We first investigated the formation and transport of small polarons; our results indicated that electron small polarons may occur in bulk Ta_3N_5, but hole polarons are not energetically favorable. However, the mobility estimated for electron small polaron hopping is orders of magnitude smaller than that reported experimentally, suggesting that the main charge transport mechanism for both electrons and holes is bandlike. Therefore, we next investigated whether substitutional impurities (Nb, V, and P) or strain may lower the carrier effective masses of bulk Ta_3N_5. We found a substantial reduction in both electron and hole effective masses (up to 17% for electrons and 39% for holes) under an applied strain of 1%–2%, which may lead, for example, to an improvement of 30% and 15% in electron and hole mobilities, respectively, for an applied biaxial strain of 1.5% (estimated considering only scattering by acoustical phonons). On the other hand, the presence of substitutional V and P atoms did not improve the band transport properties of Ta_3N_5 while the incorporation of Nb at Ta sites led to a small increase (∼6%) in the hole mobility.

The rest of the paper is organized as follows: In Sec. II we describe the details of our first-principles calculations and in Sec. III we present and discuss our results. Our conclusions are provided in Sec. IV.

II. COMPUTATIONAL DETAILS

We performed first-principles calculations based on density-functional theory (DFT) [16] using the generalized gradient approximation (GGA) proposed by Perdew, Burke, and Ernzerhof (PBE) [17] as well as DFT+U [18] and hybrid functionals. We employed the QUANTUM ESPRESSO (QE) package [19], plane-wave basis sets with an energy cutoff of

*jmmorbec@gmail.com

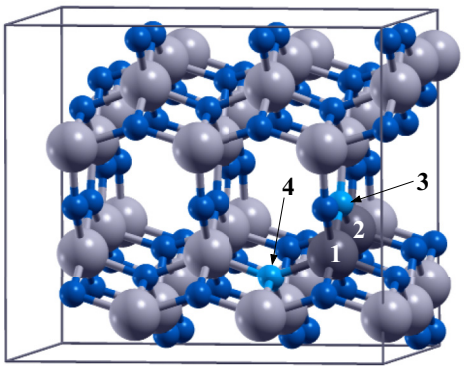

FIG. 1. Ball and stick representation of a $3 \times 1 \times 1$ supercell of Ta_3N_5 indicating the sites investigated for electron (Ta atoms 1 and 2) and hole (N atoms 3 and 4) localization. Ta and N atoms are shown as gray and blue spheres, respectively.

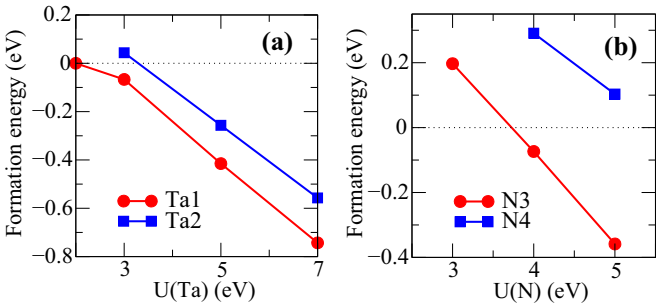

FIG. 2. Formation energy E_p of (a) electron and (b) hole small polarons in Ta_3N_5 as a function of the parameter U(Ta) for electrons and U(N) for holes (see text).

160 Ry, and norm-conserving Hartwigsen-Goedecker-Hutter (HGH) [20] pseudopotentials.

The Ta_3N_5 crystal has an orthorhombic structure (space group $Cmcm$) with 32 atoms in the conventional unit cell; our calculated lattice parameters [8] obtained with the PBE functional, $a = 3.87$, $b = 10.22$, and $c = 10.26$ Å, are in excellent agreement with the experimental values: $a = 3.89$, $b = 10.21$, and $c = 10.26$ Å [21]. To study the effects of impurities and strain on the electronic and charge transport properties of the system (Sec. III B) we used a $1 \times 1 \times 1$ supercell with 32 atoms and a $12 \times 6 \times 6$ Monkhorst-Pack grid [22]. The possible formation of small polarons in Ta_3N_5 (Sec. III A) was investigated using a $3 \times 1 \times 1$ supercell with 96 atoms (see Fig. 1) and a $3 \times 3 \times 3$ Monkhorst-Pack grid. A U parameter [18] was applied to the tantalum $5d$ and nitrogen $2p$ orbitals and different values of U were used, as discussed in Sec. III A. For calculations with hybrid functionals we used the self-consistent hybrid (sc-hybrid) [23], PBE0 [24], and Heyd-Scuseria-Ernzerhof (HSE) [25]. In this case, the k-point grid was reduced to the Γ point only and the energy cutoff was reduced to 120 Ry for computational convenience.

III. RESULTS AND DISCUSSION

A. Small polarons in Ta_3N_5

We first discuss polaronic transport. Electrons and holes moving in an ionic crystal, such as Ta_3N_5, can be trapped by electron-phonon interactions and form polarons. When the radius of this quasiparticle is of the order of the interionic distance, the trapped charge forms a so-called *small polaron* [26,27], whose transport occurs via thermally activated hopping. Small polarons are stable in various transition metal oxides considered potential photoanodes for water splitting, such as TiO_2 [28], $BiVO_4$ [29,30], and Fe_2O_3 [31], and the transport properties of these materials are affected by their presence. In nitrides, hole small polarons were found to be metastable, e.g., in AlN (0.3 eV higher in energy than the nonpolaronic configuration) and energetically stable in Mg-doped AlN and GaN [32].

As polarons originate from electron-phonon interactions, we first checked the accuracy of our calculations in reproducing the phonons of Ta_3N_5 (detailed results are presented in the Supplemental Material [33]). Within the framework of density-functional perturbation theory (DFPT) [34,35], we computed the infrared and Raman frequencies of Ta_3N_5 at the Brillouin zone center (see Table SI [33]) using PBE, and we found excellent agreement with the theoretical and experimental data of Ref. [36]. We also found that frequencies larger than 300 cm^{-1} are dominated by N displacements. We obtained phonon dispersion curves along the ΓX, ΓY, and ΓZ directions (Fig. S1 [33]) and from the slopes of linear fits to the acoustic branches near the Γ point we computed the group velocities and the elastic constants of bulk Ta_3N_5; our results are consistent with those obtained using the energy-strain method [37] (see Table SII [33]). The good agreement between our results and previous theoretical and experimental data showed that our phonon calculations are accurate.

Electron and hole polarons were simulated in bulk Ta_3N_5 by adding or removing an electron, respectively, from a $3 \times 1 \times 1$ supercell with 96 atoms (see Fig. 1), and applying a small perturbation around a selected atom in order to break the symmetry of the crystal; in particular, we prepared the system into an initial distorted configuration by increasing the bond lengths by $\sim$10% around the selected atom. We then minimized the system geometry in the presence of a uniform background, ensuring charge neutrality. For self-trapped electrons we considered inequivalent Ta atoms 1 and 2 and for hole small polarons we considered N atoms 3 and 4 (see Fig. 1). Note that N3 is bonded to three Ta atoms while N4 is connected to four Ta atoms. To check the presence of self-trapped charge we computed the difference in charge density between the optimized configuration with extra charge and a system with similar geometry without extra charge.

We first investigated the formation of small polarons in Ta_3N_5 as a function of the U parameter added to the Kohn-Sham Hamiltonian. Figure 2 shows the polaron formation energy E_p, obtained for different values of U(Ta) and U(N). $E_p = E_T^P - E_T^{NP}$ is the total-energy difference between the polaronic (E_T^P) and nonpolaronic (E_T^{NP}) configurations and negative values of E_p indicate that the polaronic configuration is energetically more stable (geometry relaxation was allowed in the calculations of both polaronic and nonpolaronic configurations). As expected, the larger the U, the stronger the charge localization and the larger E_p. Electron small polarons are

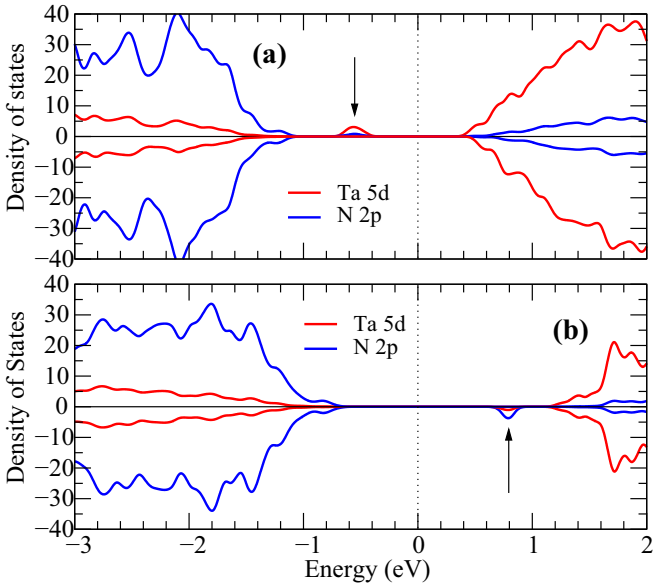

FIG. 3. Density of states of Ta_3N_5 with (a) a self-trapped electron at Ta1 [computed using $U(\mathrm{Ta}) = 7$ eV] and (b) a self-trapped hole at N3 [computed using $U(\mathrm{N}) = 5$ eV]. The zero energy is set at the Fermi level, indicated by the dotted line.

stable for $U(\mathrm{Ta}) \geqslant 3$ eV. Using $U(\mathrm{Ta}) = 7$ eV—a value which reproduces the band gap obtained in our previous work [8] using the sc-hybrid functional [23] and G_0W_0 (see Table/SIII [33])—we found that the self-trapped electrons at Ta1 and Ta2 are 0.74 and 0.56 eV more stable than the delocalized configuration, respectively. We note that a value of $U = 7$ eV is in reasonable agreement with that computed from first principles in Ref. [38] ($U = 6.47$ eV). On the other hand, as shown in Fig. 2(b), polaronic configurations are not formed for $U(\mathrm{N}) < 3$ eV and hole small polarons are energetically favorable only for $U(\mathrm{N}) \geqslant 4$ eV, a value much bigger than the one computed in Ref. [38] ($U = 0.06$ eV). The density of states of the polaronic configurations (Fig. 3), obtained using DFT + U, show the defect states associated with the electron and hole small polarons: For electrons trapped at the Ta1 site, the occupied state lies about 1.3 eV below the conduction band [Fig. 3(a)] while for holes at the N3 site the unoccupied state is ∼1.5 eV above the valence band [Fig. 3(b)].

These results point at stable electron polarons and unfavorable hole ones. However, DFT + U is known to overestimate the charge localization in some cases [39–41] and, in order to check the robustness of our results, we performed calculations using hybrid functionals, namely, sc-hybrid [23], PBE0 [24], and HSE [25]. We started from the optimized geometry for both polaronic and nonpolaronic configurations obtained with DFT + U [$U(\mathrm{Ta}) = 7$ eV and $U(\mathrm{N}) = 5$ eV] and we performed self-consistent calculations using hybrid functionals without geometry relaxation. For electron small polarons we found $E_p^{\mathrm{sc}} = 0.03$, $E_p^{\mathrm{PBE0}} = -0.07$, and $E_p^{\mathrm{HSE}} = 0.11$ eV, with sc-hybrid, PBE0, and HSE, respectively, and for hole small polarons we obtained $E_p^{\mathrm{sc}} = 0.41$, $E_p^{\mathrm{PBE0}} = 0.23$, and $E_p^{\mathrm{HSE}} = 0.46$ eV. Although the results obtained with hybrid functionals are only qualitative estimates, since we did not optimize the geometry at the respective levels of theory, several

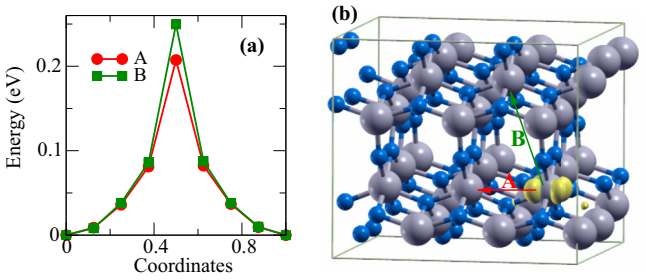

FIG. 4. (a) Energy variation for electron polaron hopping along paths A and B [shown in (b)] computed using $U(\mathrm{Ta}) = 7$ eV.

conclusions can be drawn. First, we note that hole polarons are not expected to be stable, irrespective of the functional used. The stability of the electron polaronic configurations depends on the mixing parameter α, as observed by Kweon *et al.* [30] for electron polarons in $BiVO_4$. Since, in the case of sc-hybrids, the energy of the nonpolaronic configurations was only 0.03 eV higher than the polaronic one, we investigated whether stable polarons could be found in other geometries; we considered several different configurations obtained from the linear interpolation of the geometries of the polaronic and nonpolaronic configurations, and we found some electron polaronic configurations about 70 meV more stable than the nonpolaronic one. The same procedure was performed for hole polarons, but we did not find any favorable polaronic configuration. Given the accuracy of the sc-hybrid functional in reproducing the electronic structure of Ta_3N_5 [8], these results suggest that electron small polarons may occur in bulk Ta_3N_5, with a low formation energy, and small polaron hopping transport may coexist with band transport for electrons. On the other hand, hole small polarons are not favorable and the transport mechanism for holes is bandlike.

Within an adiabatic hopping approximation, the small polaron mobility μ_{pol} can be estimated using the Einstein relation

$$\mu_{\mathrm{pol}} = \frac{eD}{k_B T} = \frac{eR^2 n}{k_B T}\nu \exp\left[-\frac{E_a}{k_B T}\right], \qquad (1)$$

where D is the diffusion coefficient, k_B is the Boltzmann constant, T is the temperature, R is the distance between transfer sites, n is the number of accepting sites, ν is the longitudinal optical phonon frequency and E_a is the activation energy. Figure 4(a) shows the barrier (or activation energy), estimated at the DFT + U level with $U(\mathrm{Ta}) = 7$ eV, to move an electron small polaron between two equivalent sites. Taking the nearest equivalent atoms to the polaron site, we considered electron polaron hopping along paths A and B, as shown in Fig. 4(b). Polaron hopping is described via Marcus theory and the intermediate configurations along the polaron transfer pathway are determined using linear interpolation between the initial and the final states. We found $E_a = 0.21$ eV along path A and $E_a = 0.25$ eV along path B, which are of a similar magnitude to those reported, e.g., for $BiVO_4$ (between 0.2 and 0.5 eV, depending on the mixing parameter α in the HSE functional) [30] and for TiO_2 (∼0.3 eV) [28]. Using the largest optical phonon frequency from our phonon calculations [33], $\nu = 2.67 \times 10^{13}$ Hz, and $T = 300$ K, we obtained $\mu_{\mathrm{pol}} \approx$

9.96×10^{-4} cm^2/V s along path A and $\mu_{pol} \approx 8.37 \times 10^{-4}$ cm^2/V s along path B. These mobilities are at least two orders of magnitude lower than the mobility measured in orthorhombic Ta_3N_5 films [12], namely, 1.0×10^{-1} cm^2/V s. Hence we conclude that electron small polaron may occur in bulk Ta_3N_5, but the main transport mechanism for electrons in this material is expected to be bandlike.

B. Effects of impurities and strain on the band transport mobilities of Ta_3N_5

We now turn to the discussion of band transport. The band transport mobility can be affected by several different scattering mechanisms, including acoustic phonons, optical phonons, and ionized impurity scattering. The carrier effective mass (m^*) is an important factor influencing all of these mechanisms; for example, the mobility due to acoustic phonon scattering [42,43] is proportional to $\frac{1}{m_I^*(m_b^*)^{3/2}}$, where $m_I^* = 3(1/m_x^* + 1/m_y^* + 1/m_z^*)^{-1}$ and $m_b^* = (m_x^* m_y^* m_z^*)^{1/3}$ are the inertial and band effective masses, respectively. Therefore, large effective masses may be responsible for low band transport mobilities. In our previous work [8] we estimated the effective masses of electrons (m_e^*) and holes (m_h^*) from quadratic fits of the band structure and we found large effective masses along some directions, e.g., $m_e^* = 2.70m_0$ and $m_h^* = 3.56m_0$ along the ΓY direction.

Here, we investigated the effects of substitutional impurities (Nb, V, and P) and strain on the electronic structure and carrier effective masses. Before doing so, we computed the elastic constants of Ta_3N_5 using the energy-strain method [44,45]; as can be seen in Table SII [33], our results are in good agreement with those calculated in Ref. [37].

We considered a $1 \times 1 \times 1$ supercell with 32 atoms. For substitutional impurities we investigated Nb and V replacing Ta atoms (Nb_{Ta} and V_{Ta}) and P replacing N atoms (P_N). We considered one and two impurities per supercell and examined different substitutional sites; the most stable configurations are shown in Fig. S2 [33]. Both atomic positions and lattice constants were allowed to relax and the optimized lattice parameters are listed in Table SIV [33].

Table I lists the band gap and the carrier effective masses in Nb_{Ta}-Ta_3N_5, V_{Ta}-Ta_3N_5, and P_N-Ta_3N_5 systems computed at the PBE level of theory. We did not find any significant improvement in the effective masses, with respect to the pristine system, that could lead to a substantial enhancement in the carrier mobilities. For low concentrations of Nb_{Ta} we found that the hole effective mass along the ΓY direction decreased by ∼3%, which may lead to an increase of ∼6% in the hole mobility due to acoustic phonon scattering (here, we are estimating changes in the mobility considering only changes in the effective masses).

Regarding the band gaps, we found a significant reduction in the band gaps in the presence of substitutional V and P atoms. For a high concentration of P_N the system becomes metallic at the PBE level of theory. For V_{Ta} we found that the band gap reduces by ∼28% and 68% with low and high impurity concentrations, respectively; this is mainly due to the presence of V $3d$ states (see Fig. S3 [33]), which have a lower energy than Ta $5d$ orbitals, at the bottom of the conduction band. A reduction of 28% due to the presence of V_{Ta} may bring the optical band gap of Ta_3N_5 (which is ∼2.1 eV [8]) close to ∼1.5 eV, which is lower than the minimum required to split water (∼1.9 eV is an optimal value [46] considering thermodynamic losses and reaction overpotentials). Therefore, our results suggest that the presence of V_{Ta} and P_N does not improve the band transport properties of Ta_3N_5, and V_{Ta}-Ta_3N_5 and P_N-Ta_3N_5 are not suitable for photoelectrochemical water splitting. On the other hand, the presence of substitutional Nb atoms in Ta_3N_5 may potentially enhance the performance of this material since it leads to a small increase in the hole mobility, keeping the band gap in the appropriate range for visible light absorption.

We next investigated the effects of strain on the band structure and carrier effective masses of Ta_3N_5 bulk. We considered the following: (i) Uniaxial strain along the a, b, and c directions [see Fig. S4(d) [33]]—the cell was strained in one direction and allowed to fully relax along the perpendicular directions. (ii) Biaxial strain in the ab, ac, and bc planes—the in-plane lattice parameters were equally strained and lattice relaxation was allowed in the direction perpendicular to the plane. (iii) Hydrostatic strain—the cell was equally strained in the a, b, and c directions. We considered strains in the range of −1.5 to 1.5%, likely to be realized experimentally since similar strains have been reported, e.g., in TiO_2 (tensile strain

TABLE I. Calculated band gaps E_g and carrier effective masses of Nb_{Ta}-Ta_3N_5, V_{Ta}-Ta_3N_5, and P_N-Ta_3N_5 with low (1 impurity/supercell, corresponding to a concentration of ∼8.3%) and high (2 impurities/supercell, corresponding to a concentration of ∼16.7%) impurity concentration. The calculations reported below are at the PBE level of theory.

		m^*/m_0 (electron/hole)		
System	E_g (eV)	ΓX	ΓY	ΓZ
Ta_3N_5	1.43	0.21/0.66	2.70/3.56	0.85/0.26
Low impurity concentration				
Nb_{Ta}-Ta_3N_5	1.32	0.24/0.66	2.70/3.46	0.92/0.26
V_{Ta}-Ta_3N_5	1.03	0.48/0.59	3.37/4.85	1.42/0.28
P_N-Ta_3N_5	0.83	0.23/0.98	3.16/4.76	0.85/0.32
High impurity concentration				
Nb_{Ta}-Ta_3N_5	1.18	0.24/0.73	2.83/3.31	0.95/0.27
V_{Ta}-Ta_3N_5	0.45	0.46/0.58	3.53/3.83	1.25/0.32
P_N-Ta_3N_5	Metallic			

up to 4% on rutile TiO_2 [47] and compressive strain about 1.83% in anatase TiO_2 nanostructures [48]), a material with elastic constants and a bulk modulus comparable to those of Ta_3N_5 [49,50]. A compressive strain of 2.7% was also achieved in $In_{0.12}Al_{0.88}N$ grown on a GaN buffer [51]; first-principles calculations at the local density approximation (LDA) level of theory predicted the bulk modulus of $In_{0.12}Al_{0.88}N$ to be between 196 and 214 GPa [52], similar to that computed for Ta_3N_5 (244 GPa) [37].

At the DFT-PBE level of theory, strain-free Ta_3N_5 bulk has an indirect band gap of 1.43 eV, with the valence band maximum (VBM) located at the Γ point and the conduction band minimum (CBM) located at the *Y* point [8]. We found that hydrostatic strains between −1.5 and 1.5% induce small changes in the band gap, less than 1.5% [see Fig. S5(c) [33]], while uniaxial strain along the *b* direction induces changes up to 5.6% [Fig. S5(a) [33]]. For biaxial strain along the *a* and *c* directions [Fig. S5(b) [33]], we found that the band gap decreases up to 6.5% under tensile strain and increases up to 6.1% with compression. These small changes in the band gap do not compromise the appropriateness of this material for water splitting, since we expect the optical band gap of strained Ta_3N_5 to be between 1.96 and 2.23 eV.

Finally, we estimated the carrier effective masses in the strained systems. We found (see Figs. S6, S7, and S8 [33]) that the effective masses of both electrons and holes significantly change. Under a compressive uniaxial strain of 1.5% along the *b* direction, for example, we found a reduction up to ∼26% in the hole effective mass and up to ∼13% in the electron effective mass. We estimate that the reduction in the effective masses may lead to an increase of ∼33% and ∼8% in the electron and hole mobility, respectively, due to acoustic phonon scattering. In the case of biaxial strain, we estimated that the reduction of ∼16% in the electron effective mass under 1.5% tensile strain along the *a* and *c* directions may result in an improvement of 31% in the electron mobility, while an increase up to 15% in the hole mobility can be achieved under compressive strain along the *b* and *c* directions. Our results therefore suggest that the band transport properties of Ta_3N_5 can be improved by straining the material.

IV. CONCLUSIONS

In summary, we performed first-principles calculations to investigate the charge transport properties of bulk Ta_3N_5. We investigated the formation of small polarons using both DFT + *U* and hybrid functionals and we found that electron small polarons may occur, while hole small polarons are not stable. The computed electronic small polaron mobilities are at least two orders of magnitude smaller than measured mobilities [7,12], suggesting that polaron transport may coexist with band transport but it is not the main transport mechanism for electrons. Hence, our results indicate that band transport is the main transport mechanism for both electrons and holes in Ta_3N_5. We also showed that the overall large effective masses of electrons and holes may be reduced with applied strain. In particular, electron mobility may be increased by ∼30% and hole mobility by 15% under moderate biaxial strains in the range of −1.5 to 1.5%.

ACKNOWLEDGMENTS

This work was supported by the National Science Foundation (NSF) under the NSF Center for Solar fuels (NSF-CHE-1305124). This research used resources of the National Energy Research Scientific Computing Center, which is supported by the Office of Science of the US Department of Energy under Contract No. DE-AC02-05CH11231. We thank Hosung Seo, Nicholas Brawand, Matthew Goldey, Yuping He, Márton Vörös, and Ieva Narkeviciute for useful discussions.

[1] B. A. Pinaud, A. Vailionis, and T. F. Jaramillo, Chem. Mater. **26**, 1576 (2014).
[2] A. Dabirian and R. van de Krol, Appl. Phys. Lett. **102**, 033905 (2013).
[3] W.-J. Chun, A. Ishikawa, H. Fujisawa, T. Takata, J. N. Kondo, M. Hara, M. Kawai, Y. Matsumoto, and K. Domen, J. Phys. Chem. B **107**, 1798 (2003).
[4] Y. Li, T. Takata, D. Cha, K. Takanabe, T. Minegishi, J. Kubota, and K. Domen, Adv. Mater. **25**, 125 (2013).
[5] A. Ishikawa, T. Takata, J. N. Kondo, M. Hara, and K. Domen, J. Phys. Chem. B **108**, 11049 (2004).
[6] B. A. Pinaud, P. C. K. Vesborg, and T. F. Jaramillo, J. Phys. Chem. C **116**, 15918 (2012).
[7] A. Ziani, E. Nurlaela, D. S. Dhawale, D. A. Silva, E. Alarousu, O. F. Mohammed, and K. Takanabe, Phys. Chem. Chem. Phys. **17**, 2670 (2015).
[8] J. M. Morbec, I. Narkeviciute, T. F. Jaramillo, and G. Galli, Phys. Rev. B **90**, 155204 (2014).
[9] D. Yokoyama, H. Hashiguchi, K. Maeda, T. Minegishi, T. Takata, R. Abe, J. Kubota, and K. Domen, Thin Solid Films **519**, 2087 (2011).
[10] Y. He and G. Galli, Chem. Mater. **26**, 5394 (2014).
[11] Y. Wang, Y. Zhang, P. Zhang, and W. Zhang, Phys. Chem. Chem. Phys. **17**, 11516 (2015).
[12] M. Respinis, M. Fravventura, F. F. Abdi, H. Schreuders, T. J. Savenije, W. A. Smith, B. Dam, and R. van de Krol, Chem. Mater. **27**, 7091 (2015).
[13] S. S. Shinde, R. A. Bansode, C. H. Bhosale, and K. Y. Rajpure, J. Semicond. **32**, 013001 (2011).
[14] H. Tang, K. Prasad, R. Sanjinès, P. E. Schmid, and F. Lévy, J. Appl. Phys. **75**, 2042 (1994).
[15] F. F. Abdi, T. J. Savenije, M. M. May, B. Dam, and R. van de Krol, J. Phys. Chem. Lett. **4**, 2752 (2013).
[16] P. Hohenberg and W. Kohn, Phys. Rev. **136**, B864 (1964).
[17] J. P. Perdew, K. Burke, and M. Ernzerhof, Phys. Rev. Lett. **77**, 3865 (1996); **78**, 1396 (1997).
[18] V. I. Anisimov, J. Zaanen, and O. K. Andersen, Phys. Rev. B **44**, 943 (1991); V. I. Anisimov, I. V. Solovyev, M. A. Korotin, M. T. Czyzyk, and G. A. Sawatzky, *ibid.* **48**, 16929 (1993); A. I. Liechtenstein, V. I. Anisimov, and J. Zaanen, *ibid.* **52**, R5467(R) (1995).

[19] P. Giannozzi, S. Baroni, N. Bonini, M. Calandra, R. Car, C. Cavazzoni, D. Ceresoli, G. L. Chiarotti, M. Cococcioni, I. Dabo, A. Dal Corso, S. Fabris, G. Fratesi, S. de Gironcoli, R. Gebauer, U. Gerstmann, C. Gougoussis, A. Kokalj, M. Lazzeri, L. Martin-Samos, N. Marzari, F. Mauri, R. Mazzarello, S. Paolini, A. Pasquarello, L. Paulatto, C. Sbraccia, S. Scandolo, G. Sclauzero, A. P. Seitsonen, A. Smogunov, P. Umari, and R. M. Wentzcovitch, J. Phys.: Condens. Matter **21**, 395502 (2009).

[20] C. Hartwigsen, S. Goedecker, and J. Hutter, Phys. Rev. B **58**, 3641 (1998).

[21] N. E. Brese, M. O'Keeffe, P. Rauch, and F. J. DiSalvo, Acta Crystallogr., Sect. C **47**, 2291 (1991).

[22] H. J. Monkhorst and J. D. Pack, Phys. Rev. B **13**, 5188 (1976).

[23] J. H. Skone, M. Govoni, and G. Galli, Phys. Rev. B **89**, 195112 (2014).

[24] C. Adamo and V. Barone, J. Chem. Phys. **110**, 6158 (1999).

[25] J. Heyd, G. E. Scuseria, and M. Ernzerhof, J. Chem. Phys. **118**, 8207 (2003); **124**, 219906 (2006).

[26] I. G. Austin and N. F. Mott, Adv. Phys. **50**, 757 (2001).

[27] D. Emin, Phys. Today **35** (6), 34 (1982).

[28] N. A. Deskins and M. Dupuis, Phys. Rev. B **75**, 195212 (2007).

[29] K. E. Kweon and G. S. Hwang, Phys. Rev. B **86**, 165209 (2012).

[30] K. E. Kweon, G. S. Hwang, J. Kim, S. Kim, and S. Kim, Phys. Chem. Chem. Phys. **17**, 256 (2015).

[31] N. Iordanova, M. Dupuis, and K. M. Rosso, J. Chem. Phys. **122**, 144305 (2005).

[32] J. L. Lyons, A. Janotti, and C. G. Van de Walle, J. Appl. Phys. **115**, 012014 (2014).

[33] See Supplemental Material at http://link.aps.org/supplemental/10.1103/PhysRevB.93.035201 for details about phonon calculations, effects of impurities and strain on the electronic structure and effective masses, and band gaps for different values of U.

[34] P. Giannozzi, S. de Gironcoli, P. Pavone, and S. Baroni, Phys. Rev. B **43**, 7231 (1991).

[35] S. Baroni, S. de Gironcoli, A. Dal Corso, and P. Giannozzi, Rev. Mod. Phys. **73**, 515 (2001).

[36] E. Nurlaela, M. Harb, S. del Gobbo, M. Vashishta, and K. Takanabe, J. Solid State Chem. **229**, 219 (2015).

[37] J. Wang, J. Feng, L. Zhang, Z. Li, and Z. Zou, Phys. Chem. Chem. Phys. **16**, 15375 (2014).

[38] J. Wang, T. Fang, L. Zhang, J. Feng, Z. Li, and Z. Zou, J. Catal. **309**, 291 (2014).

[39] J. M. Garcia-Lastra, J. S. G. Myrdal, R. Christensen, K. S. Thygesen, and T. Vegge, J. Phys. Chem. C **117**, 5568 (2013).

[40] In Ref. [39] Garcia-Lastra *et al.* investigated the formation of small polarons in Li_2CO_3 and they found large differences between the polaron formation energies obtained using DFT + U, −5.17 eV for holes and −0.80 eV for electrons, and HSE, −0.42 eV for holes and −0.05 eV for electrons.

[41] H. Ding, H. Lin, B. Sadigh, F. Zhou, V. Ozolins, and M. Asta, J. Phys. Chem. C **118**, 15565 (2014).

[42] H. Wang, Y. Pei, A. D. LaLonde, and G. J. Snyder, Proc. Natl. Acad. Sci. USA **109**, 9705 (2012).

[43] Y. I. Ravich, B. A. Efimova, and V. I. Tamarchenko, Phys. Status Solidi B **43**, 11 (1971).

[44] P. Ravindran, L. Fast, P. Korzhavyi, B. Johansson, J. Wills, and O. Eriksson, J. Appl. Phys. **84**, 4891 (1998).

[45] P. W. O. Nyawere, N. W. Makau, and G. O. Amolo, Physica B **434**, 122 (2014).

[46] Y. Ping, D. Rocca, and G. Galli, Chem. Soc. Rev. **42**, 2437 (2013).

[47] D. V. Potapenko, Z. Li, J. W. Kysar, and R. M. Osgood, Nano Lett. **14**, 6185 (2014).

[48] N. Rahmani and R. S. Dariani, Superlattices Microstruct. **85**, 504 (2015).

[49] From phonon calculations and using the PW91 functional, Shojaee *et al.* [50] found $C_{11} = C_{22} = 333$, $C_{33} = 198$, $C_{44} = C_{55} = 39$, $C_{66} = 57$–60 GPa for anatase and $C_{11} = C_{22} = 269$, $C_{33} = 506$, $C_{44} = C_{55} = 105$, $C_{66} = 217$ GPa for rutile TiO_2, while we obtained $C_{11} = 309.39$, $C_{22} = 324.71$, $C_{33} = 317.50$, $C_{44} = 101.84$, $C_{55} = 115.69$, and $C_{66} = 44.98$ GPa for Ta_3N_5 at the PBE level of theory [33]. The bulk moduli of rutile and anatase TiO_2 obtained using LDA (241 and 187 GPa, respectively) [50] and PW91 (201 and 173 GPa, respectively) [50] are also similar to that computed for Ta_3N_5 (244 GPa) using PBE [37].

[50] E. Shojaee and M. R. Mohammadizadeh, J. Phys.: Condens. Matter **13**, 015401 (2010).

[51] E. Jones, D. Cooper, J.-L. Rouviere, A. Béché, M. Azize, T. Palacios, and Silvija Gradečak, Appl. Phys. Lett. **103**, 231904 (2013).

[52] Z. Dridi, B. Bouhafs, and P. Ruterana, New J. Phys. **4**, 94 (2002).